Chemistry & Biology, Vol. 11, 1553–1559, November, 2004, ©2004 Elsevier Ltd. All rights reserved. DOI 10.1016/j.chembiol.2004.08.022

Bacterial Biosynthesis of Cadmium Sulfide Nanocrystals

Rozamond Y. Sweeney,[1] Chuanbin Mao,[2,3] Xiaoxia Gao,[3] Justin L. Burt,[3] Angela M. Belcher,[1,2,4,5,6] George Georgiou,[1,3,4] and Brent L. Iverson[1,2,4,*]

[1]Institute for Cellular and Molecular Biology
[2]Department of Chemistry and Biochemistry
[3]Department of Chemical Engineering
[4]Center for Nano- and Molecular Science and Technology
[5]Texas Materials Institute
University of Texas
Austin, Texas 78712

Summary

Semiconductor nanocrystals, which have unique optical and electronic properties, have potential for applications in the emerging field of nanoelectronics. To produce nanocrystals cheaply and efficiently, biological methods of synthesis are being explored. We found that *E. coli*, when incubated with cadmium chloride and sodium sulfide, have the capacity to synthesize intracellular cadmium sulfide (CdS) nanocrystals. The nanocrystals are composed of a wurtzite crystal phase with a size distribution of 2–5 nm. Nanocrystal biosynthesis increased about 20-fold in *E. coli* cells grown to stationary phase compared to late logarithmic phase. Our results highlight how different genetic and physiological parameters can enhance the formation of nanocrystals within bacterial cells.

Introduction

Semiconductor nanocrystals have diverse practical applications, including fluorescent biological labels [1, 2] and optoelectronic transistor components [3]. The optical and electronic properties of nanocrystals are dependent on physical properties, such as particle size distribution, shape, and crystallinity. Therefore, the challenge in semiconductor nanocrystal synthesis is to precisely control these properties by manipulating synthetic parameters [4]. Many conditions of nanocrystal growth, including solvent, temperature, and precursor molecules, have been manipulated in order to enable the formation of crystals with desired properties. Particular attention has been focused on using different capping agents in an effort to control the size, shape, and crystallinity of developing nanocrystals. A variety of methods for synthesizing nanocrystals, including using biological molecules as capping agents, have been pursued. At this point, it is still difficult to predict how changing different parameters of nanocrystal synthesis will affect the physical properties of the resulting material [5].

Living organisms have the endogenous ability to exquisitely regulate synthesis of inorganic materials, such as sea shells [6], bone, teeth, and even magnetite crystals [7]. Because of this ability to precisely direct the shape and crystallinity of a developing inorganic material, there is great interest in exploiting both living organisms and biological molecules for inorganic materials synthesis. For example, amino acids, fatty acids, and polyphosphates are all biologically derived capping agents that have been used to template the growth of semiconductor nanocrystals. Early synthetic work exploited polyphosphate in aqueous solution as a capping agent for CdS nanocrystals [8, 9]. Glutathione and cysteine, thiolates that are able to form high-affinity metal ligand clusters, have been shown to promote the formation of CdS and ZnS nanocrystals [10–13]. Further control over nanocrystal synthesis has been gained by using fatty acids, which have been found to promote the synthesis of CdSe, CdS, and CdTe nanocrystals [14]. By varying the ratio of different fatty acid chain lengths, shape control of nanocrystals has been achieved [15].

Biological approaches to nanocrystal synthesis have been extended to intact biological particles. Viral scaffolds can template the nucleation and assembly of inorganic materials. For example, cowpea chorotic mottle virus and cowpea mosaic virus have been used as nucleation cages for the mineralization of inorganic materials [16, 17], and tobacco mosaic virus has been shown to direct successfully the mineralization of PbS and CdS crystalline nanowires [18]. Taking the idea one step further, peptides capable of nucleating nanocrystal growth have been identified from combinatorial screens and displayed on the surface of M13 bacteriophage. The genetically engineered phage promoted the synthesis of crystalline nanowires, and the displayed peptides showed exquisite regulation of material composition, size, and shape [19–21].

In addition to viruses, live yeast cells have been used to promote CdS nanocrystal synthesis [22]. In the presence of heavy metal stress, yeast cells increase cellular pools of glutathione and glutathione-like compounds called phytochelatins [23, 24]. The resulting metal thiolate complex formation neutralizes the toxicity of heavy metal ions and traps them inside the cell [25, 26]. Sulfide anions are readily incorporated into these cadmium-glutathione complexes, resulting in the formation of nanocrystals [27, 28].

While prokaryotic cells have been employed as templates for material nucleation or to induce precipitation of metal complexes including CdS, there are no reports of nanocrystal formation in bacteria [29–31]. However, magnetotactic bacteria synthesize chains of iron oxide and iron sulfide crystals, which have diameters that range from 35 to 120 nm precluding quantum confinement effects [7, 32]. Additionally, a strain of *Pseudomonas stutzeri*, isolated from a silver mine, produced crystals of crystalline silver and silver sulfide that range in diameter from tens to hundreds of nanometers [33]. Here, we report that *E. coli*, incubated with cadmium chloride and sodium sulfide, spontaneously form semi-

*Correspondence: biverson@mail.utexas.edu
[6]Present address: Department of Materials Science and Engineering and Division of Biological Engineering, Massachusetts Institute of Technology, Cambridge, Massacusetts 02139.

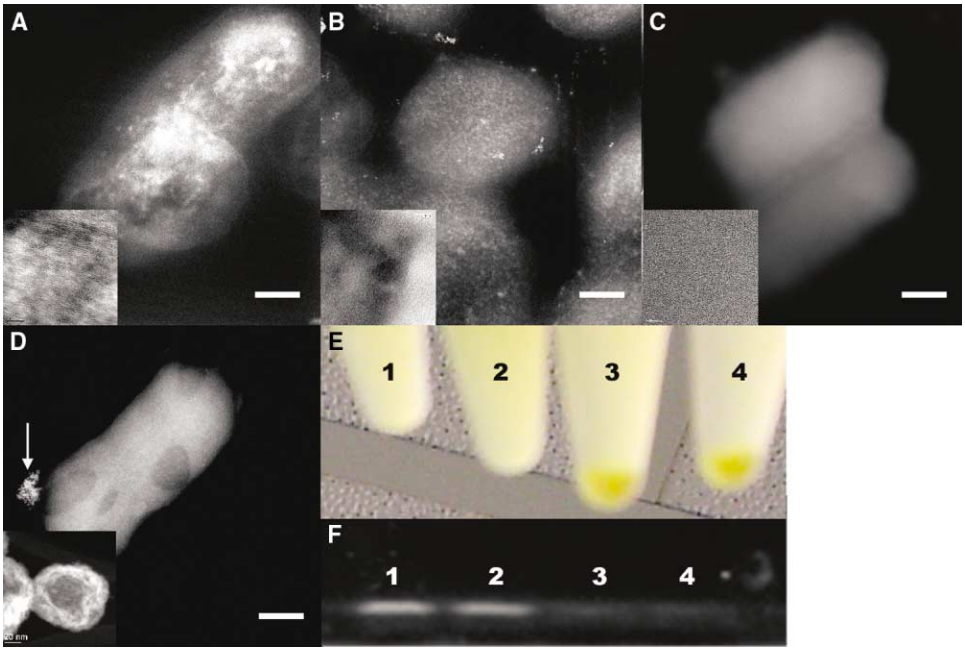

Figure 1. Nanocrystal Synthesis Is Growth Phase Dependent

STEM images of 60 nm cross-sections of nucleated *E. coli* ABLE C cells. Scale bar indicates 200 nm. Inset: HRTEM images of an intact, nucleated cell. Scale bar indicates 5 nm.

(A) Stationary phase *E. coli* ABLE C displaying a high density of intracellular crystals. Individual nanocrystals are difficult to distinguish (inset).
(B) Late log phase *E. coli* ABLE C showing only a few areas of high atomic density. Individual nanocrystals are visible by HRTEM (inset).
(C) Mid-logarithmic phase *E. coli* ABLE C cells that show no detectable nanocrystals by STEM or HRTEM.
(D) STEM image of stationary phase *E. coli* ABLE C cells incubated with precipitated CdS. Intracellular CdS is not visible, although precipitated material is sometimes seen extracellularly. Inset: STEM image of a typical CdS precipitate. Scale bar indicates 20 nm.
(E) Tubes of *E. coli* ABLE C cells after incubation with cadmium chloride and sodium sulfide. Tubes 1 and 2 (both stationary phase cells) have less precipitated CdS than Tubes 3 and 4 (both logarithmic phase cells).
(F) SDS-PAGE gel of nucleated *E. coli* ABLE C cells. Lanes 1 and 2 (both stationary phase cells) have a band corresponding to CdS nanocrystals. Lanes 3 and 4 (both logarithmic phase cells) show very faint bands, indicating significantly fewer nanocrystals.

conductor nanocrystals. Our results suggest that the processes mediating the capping and controlled growth of nanocrystals are thus intrinsic to bacterial cells. We further show that the formation of nanocrystals is markedly affected by physiological parameters, namely entry to stationary phase.

Results

Nanocrystal Formation in *E. coli* Is Growth Phase Dependent

We used scanning transmission electron microscopy (STEM) to evaluate nanocrystal formation in *E. coli* ABLE C. STEM enabled higher resolution imaging of thick, biological specimens than was possible with conventional TEM. Nanocrystal formation at different growth stages, namely, stationary, late logarithmic, and mid-logarithmic phase, was compared. Cells were incubated with 1 mM cadmium chloride, followed by the addition of sodium sulfide (1 mM) to induce nanocrystal formation. After 2 hr of incubation, the cells were cross-sectioned into 60 nm thick slices and imaged by STEM.

Nanocrystal formation was found to vary dramatically depending on the growth phase of the cells. Cross-sectioned stationary phase cells were densely packed with nanocrystals, which stabilize the cells under the electron beam (Figure 1A), presumably because high atomic density elements provide resistance to radiative damage [34]. In contrast, cross-sections of late logarithmic cells indicate sparsely packed nanocrystals inside the cells (Figure 1B). We estimated that there are, on average, 50 nanocrystals per cross-sectioned late log phase cell. An accurate determination of the number of nanocrystals per cross-section in stationary phase cells is difficult due to the dense packing of the nanocrystals. We estimated that there are $>$1000 nanocrystals per cross-sectioned stationary phase cell, which translates to $>$10,000 nanocrystals for an entire cell. Thus, the quantitative analysis of the STEM and HRTEM images indicated at least a 20-fold increase in nanocrystal formation in stationary phase cells compared to late logarithmic phase cultures. Nanocrystals were not detected in mid-logarithmic phase cells (Figure 1C).

Figures 1D and 1E further confirm the stationary phase dependence of nanocrystal formation. Figure 1D is an image of *E. coli* ABLE C cells at different growth stages, normalized by optical density, and after incubation with cadmium chloride and sodium sulfide. Tube 1 (stationary phase cells after 20 hr of growth) and Tube 2 (stationary phase cells after 16 hr of growth) have only small amounts of CdS precipitation. In contrast, Tube 3 (mid-logarithmic phase cells after 8 hr of growth) and Tube 4 (early logarithmic phase cells after 4 hr of growth) have considerably more bulk-precipitated CdS. CdS precipi-

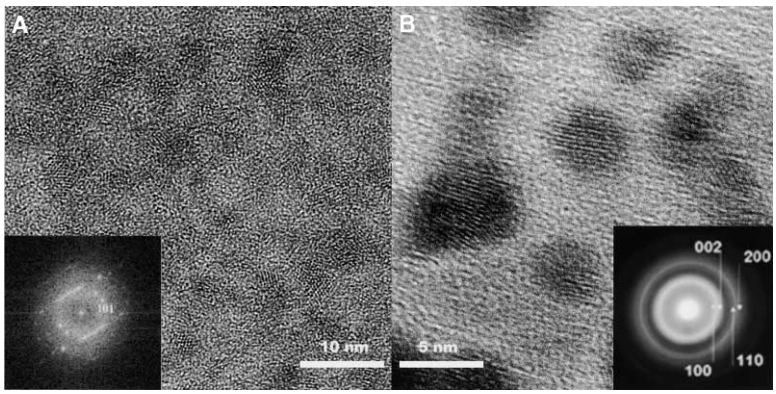

Figure 2. Nanocrystals Are Wurtzite Crystal Phase and Polydisperse Sized

(A) High-resolution TEM image of a stationary phase *E. coli* ABLE C cell. Nanocrystals are closely packed within the cell, making individual crystals difficult to distinguish. Inset: lattice imaging confirms that the particles are wurtzite.

(B) High-resolution TEM image of bacterial osmotic shockate. Discrete, polydisperse-sized nanocrystals are visible. Inset: electron diffraction pattern of the nanocrystals, indicating polycrystalline wurtzite CdS.

tation is inversely proportional to nanocrystal formation. We found that the nanocrystals migrated as a single fluorescent band on SDS-PAGE (Figure 1E). HRTEM analysis of the eluted gel slice indicates that this band is composed of CdS nanocrystals (data not shown). The difference in the intensity of the nanoparticle band from cells harvested in logarithmic and stationary phase is consistent with the estimated density of nanoparticles from the STEM analysis (Figure 1E). Conversely, the very faint band on the gel and the appearance of a precipitate in the mid-log and early log-phase cultures are consistent with external bulk precipitation and lack of nanocrystal formation.

The CdS nanocrystals appear to be forming inside the stationary phase bacterial cells. Formally, CdS nanocrystals could end up inside the bacterial cells in at least two different ways, which are not mutually exclusive. The nanocrystals could first form outside the cells, followed by transport inside during stationary phase. Alternatively, the nanocrystals could form inside the cells following transport of the Cd^{2+} and S^{2-} ions. In an attempt to distinguish between these two possibilities, $CdCl_2$ and Na_2S were incubated as before but without bacterial cells. Stationary phase *E. coli* ABLE C cells were then incubated with the preformed CdS particles before preparation of TEM samples. STEM data revealed no CdS particles present inside these cells (Figure 1D), but rather a heterogeneous precipitate associated with the outer cellular surface. This result indicates that preformed CdS nanocrystals are not likely to be associated with the cells following formation in the extracellular medium. Nonetheless, the possibility of some transport during intermediate stages of external CdS particle formation cannot be rigorously ruled out.

The Nanocrystals Are Wurtzite Crystal Phase and Polydisperse Size Distribution

Nanocrystals from stationary phase *E. coli* ABLE C cells were characterized with respect to the chemical composition, size distribution, and internal structure of the particles. For these studies, the nonaggregated nanocrystals were released from the cell by the osmotic shock procedure [42], which helped remove aggregated material that remained in the cell pellet (data not shown). High-resolution transmission electron microscopy (HRTEM) and lattice imaging reveal that the nanocrystals are wurtzite with a d spacing of 3.16 nm, corresponding to the (101) plane of wurtzite CdS (Figure 2A). The nanocrystals have a size distribution of 2–5 nm, and electron diffraction (ED) patterns confirm the wurtzite crystal structure (Figure 2B).

Nanocrystal Composition

STEM and energy dispersive spectroscopy (EDS) analysis of cross-sectioned stationary phase *E. coli* cells were used to record the elemental composition of particles within the cell. STEM analysis identified high atomic density, nanocrystal-rich regions, spherical or elliptical in shape and 1–5 μm in diameter, the same size and shape as *E. coli* cells (Figure 3A). EDS, which plotted the elemental composition of nanocrystal-rich regions, revealed that, in addition to cadmium and sulfur, the regions of densely packed nanocrystals are also rich in phosphorus, nitrogen, iron, and oxygen (Figures 3B–3H). Since the nanocrystals are colocalized with the biological elements in the cross-sectioned samples, these data further indicate that nanocrystals are synthesized within the interior of the cells, as opposed to crystallization on the surface. We note that the cadmium and sulfur signals do not correspond to every nanocrystal on the STEM image. EDS signal results from the electron beam dislodging an inner shell electron, a relatively rare event that results in the emission of characteristic X-rays. In contrast, STEM images result from the electron beam interacting directly with the nucleus. Consequently, we feel it is not surprising that each individual nanocrystal seen in a STEM image does not produce an EDS signal.

Nanocrystal Formation Parameters

Four laboratory *E. coli* strains were tested with STEM and HRTEM imaging for their ability to synthesize CdS nanocrystals. Using the same nucleation procedure as above, stationary-phase cells were imaged with HRTEM and STEM. In addition to *E. coli* ABLE C cells, *E. coli* TG1 also produced nanocrystals at a similar density. On the other hand, strains (e.g., *E. coli* RI89 and *E. coli* DH10B) did not detectably synthesize nanocrystals at any growth stage (data not shown). These results indicate that genetic differences among strains can strongly affect the ability to nucleate nanocrystals. We are currently carrying out a more comprehensive analysis of the genetic factors underlying nanocrystal formation.

Work on yeast nanocrystal biosynthesis indicated that thiols mediate crystal growth because cysteine-rich peptides were found to stabilize the surface of biosyn-

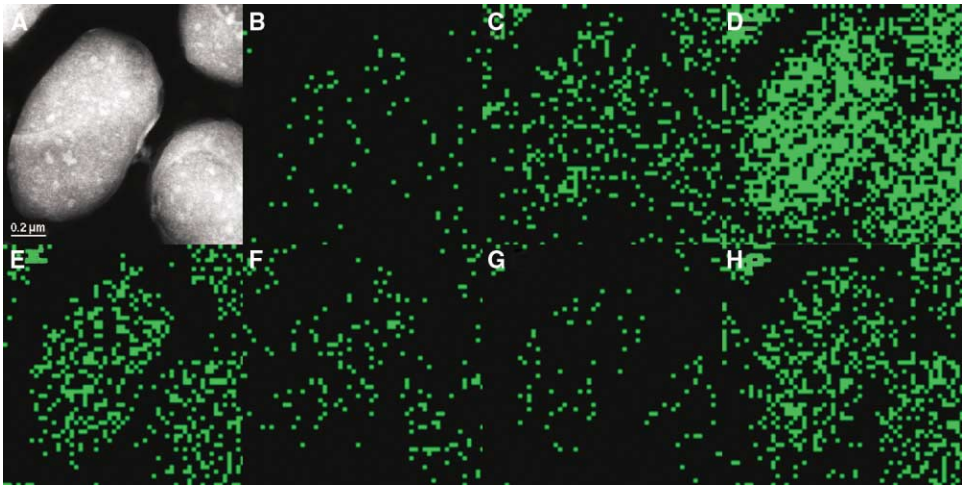

Figure 3. Elemental Mapping of a Nucleated Cell Indicates that the Nanocrystals Are Synthesized Intracellularly

(A) STEM reference image of a cross-sectioned *E. coli* ABLE C cell. Scale bar indicates 200 nm. White points indicate material of high atomic number. The images (B–H) are EDS mapping images of cross-sectioned nucleated *E. coli* ABLE C. Each panel represents detection of a different element: cadmium (B), sulfur (C), carbon (D), nitrogen (E), phosphorus (F), iron (G), and oxygen (H).

thesized CdS nanocrystals [22]. We hypothesized that, in *E. coli*, cellular thiol content in general and glutathione content in particular might be responsible for the observed growth phase dependence of nanocrystal formation. We attempted to correlate cellular thiol content with nanocrystal formation. First, analysis of free thiols with DTNB (5-5′-dithiobis-2-nitrobenzoate) [35] in cell lysates found twice as much accessible, reduced thiols in stationary phase cells compared to mid-logarithmic phase cells (Figure 4A). In addition, stationary phase cells were found to contain somewhat higher total glutathione than mid-log phase cells (Figure 4B). Finally, elemental analysis indicated that stationary phase cells have about twice the total sulfur as mid-log phase cells, consistent with the previous two results (Figure 4C). Similarly, the four strains (*E. coli* ABLE C, *E. coli* TG1, *E. coli* DH10B, and *E. coli* RI89) were found to have similar levels of cellular thiols, and the differences observed did not correlate with CdS nanocrystal formation ability (Figure 4D). The bottom line is that cellular thiol content may play a role but does not determine nanocrystal formation ability in different *E. coli* strains and growth phase.

Discussion

Previously, semiconductor nanocrystal formation had been reported only in yeast and in filamentous fungi [22, 36, 37]. Our data now suggest that *E. coli* bacteria also have the intrinsic ability to direct the synthesis of CdS nanocrystals. In particular, certain strains of *E. coli* were shown to contain polydisperse, wurtzite CdS nanocrystals that are 2–5 nm in size. Control experiments with preformed CdS particles indicated that the nanocrystals are not formed outside and then transported into the cells. Rather, the nanoparticles are apparently being formed inside bacterial cells following transport of Cd^{2+} and S^{2-} ions.

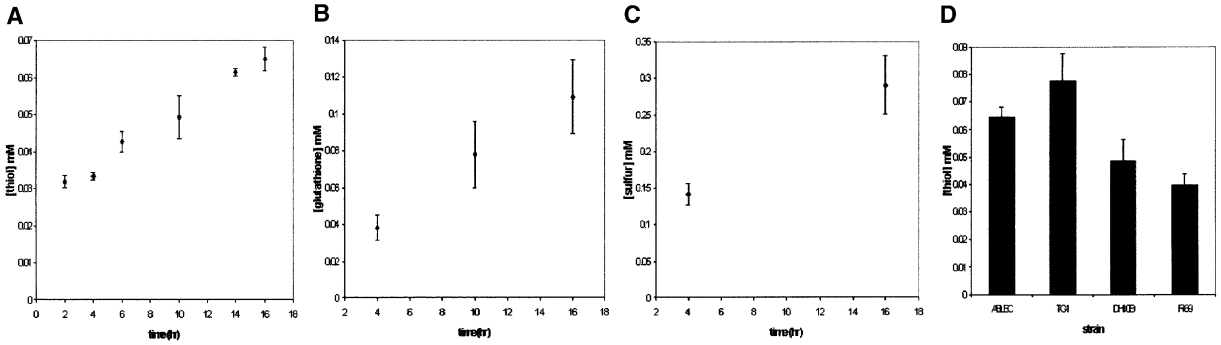

Figure 4. Cellular Thiol Content and Cadmium Uptake Increase as the Cell Enters Stationary Phase

(A) Plot of the cellular concentration of free, reduced thiols versus time of cell culture growth.

(B) Plot of total cellular glutathione versus growth time.

(C) Plot of total cellular sulfur content versus growth time.

(D) The concentration of free reduced thiols in four different *E. coli* strains at stationary phase. The y axis for each plot indicates concentration from a cell lysate solution of 4×10^9 cells diluted in 1 ml buffer.

The presence of cellular nanocrystals was strongly dependent on the strain used as well as the growth phase of the cells and occurred predominantly in stationary phase. Attempts were made to correlate these observations with the amount of free thiol and the amount of glutathione present in the cells. Although these parameters may contribute, no trend emerged that adequately predicted nanocrystal formation.

Bacteria adapt to stationary phase by changing the expression patterns of numerous genes, including increasing transcription levels of nearly 1500 genes [38]. Interestingly, the synthesis of fatty acids, known to serve as in vitro biological nanocrystal templating agents, is not increased in stationary phase [38]. On the other hand, the synthesis of polyphosphate, another in vitro nanocrystal capping agent, increases at stationary phase and may possibly act as a nanocrystal templating agent [39, 40].

Understanding the genetic and physiological factors that underlie nanocrystal formation in *E. coli* may ultimately enable manipulation of microbially derived nanocrystal production. For example, inorganic synthesis employs different ratios of multiple capping agents in order to synthesize nanocrystals of various shapes, such as rods or stars. By controlling the synthesis and relative amounts of small thiols, polyphosphates, and fatty acids in *E. coli*, it may someday be possible to control the crystallinity, shape, size distribution, and optical properties of nanocrystals in unprecedented ways.

Significance

To our knowledge, this is the first report of semiconductor nanocrystal synthesis in bacteria. We demonstrate that *E. coli* has the endogenous ability to direct the growth of semiconductor nanocrystals, and we find that parameters such as growth phase and strain type are essential for initiating nanocrystal growth. *E. coli* represents a simple yet powerful prokaryotic genetic system with the potential to elucidate the key features of nanocrystal synthesis in living cells. By understanding parameters of nanocrystal synthesis in microbes, it might be possible to modulate the properties of biosynthesized nanocrystals, such as size, shape, and crystal structure.

Experimental Procedures

Nanocrystal Nucleation

E. coli strains **ABLE C** ((lacZ$^-$) [Kan^r, mcrA$^-$, mcrCB$^-$, mcrF$^-$, mrr$^-$, hsdR($r_K^-m_K^-$)] [F′proAB, lacI^q,ZD M15, Tn10(Tet^r)]); **TG1** (supE, thi-1, D(lac-proAB), D(mcrB-hsdSM)5, ($r_K^-m_K^-$), [F′ traD36, proAB, lacI^q D M15]); **RI89** (MC1000 phoR Dara714 leu$^+$); and **DH10B** (F-mcrA del (mrr-hsdRMS-mcrBV) phi80 lacZdelM15 del lacX74 deoR recA1endA1 araD139 del(ara,leu)7697 galU galK lambda-rpsL nupG) were used for our experiments. A single colony was picked from an agar plate and grown at 37°C with shaking in LB. The overnight culture was diluted 1/100 into fresh media. Cells were harvested a various time points. After a minimum of 16 hr of growth, the cells were no longer dividing, and the optical density (OD) at 600 nm was approximately 5.0. The culture was considered to be in stationary phase. After about 10 hr of growth, the culture was close to but had not yet reached saturation, and the OD_{600nm} was around 4.0. These cells were considered to be in late logarithmic phase. Mid-logarithmic phase cells were harvested after 4 hr of growth when the cells were dividing exponentially, and the OD_{600nm} was about 0.6. Nanocrystal formation was initiated by adding $CdCl_2$ (1 mM) to a cell sample suspended in phosphate-buffered saline (PBS) (10 mM phosphate [pH 7.2], 0.8% NaCl). The cells were incubated for 20 min at 25°C before the slow addition of freshly prepared sodium sulfide (1 mM). The samples were incubated at room temperature with end-over-end rotation. After 1.5 hr, the solution was spun at 3000 rpm for 10 min. The pellet was resuspended in PBS with 2% glutaraldehyde and incubated at room temperature for 2 hr. The cell pellet was washed once with PBS before undergoing dehydration in graded alcohols (30%, 50%, 70%, 90%, 98%, absolute ethanol, 15 min each step). The cells were spun at 3000 rpm for 10 min, and the pellet was resuspended in LR White Medium Grade embedding resin. Cells were incubated in this solution for 30 min. The cells were then centrifuged at 3000 rpm and resuspended in LR White Medium Resin with added accelerant/catalyst, following the manufacturer's instructions. The solution was poured into molds and allowed to harden overnight at 60°C. The hardened pellets were cut into 60 nm thin slices with an ultramicrotome. The slices were floated on water and placed on a carbon-coated copper TEM grid.

SDS-PAGE Gel Electrophoresis

E. coli cells harvested at different growth stages were normalized to $OD_{600} = 6.0$. The cells were nucleated with CdS as described above. Then, the cells were lysed by two passages though a French pressure cell. The lysate was spun briefly (2 min, 3000 rpm) to remove precipitated CdS. The supernatant was mixed at a 1:1 ratio with SDS-PAGE loading dye containing 5% β-mercaptoethanol. The mixture was electrophoresed on a 16% Tris-Tricine gel at 80 V for 1 hr. The gel was imaged on a UV light box. Nanocrystals can be removed by soaking the gel band slice in ddH_2O overnight and then filtering the solution to remove excess polyacrylamide.

Osmotic Shock

Osmotic shock was induced using a published procedure [41]. This procedure released nanocrystals from the cell and allowed us to make TEM samples of cellular nanocrystals without excess contamination from the bulk of cellular components. Briefly, cells were suspended in a sucrose/lysozyme solution (0.75 M sucrose, 0.1 M Tris [pH 7.5], 10 μg/ml lysozyme). Next, a solution of EDTA was added (1 mM EDTA [pH 7.5]). The cells were incubated at 0°C for 10 min before magnesium chloride (0.5 M) was added. The cells were centrifuged and the supernatant was collected. The supernatant was dialyzed and transferred to carbon-coated copper TEM grids for characterization.

Glutathione-HPLC Assay

This assay was performed as described previously [42]. Cells were harvested at various times and suspended in PBS to $OD = 4.0$. Proteins were precipitated from the cell lysate by addition of 5-sulfosalicylic acid, and N-ethylmorpholine was added as a thiol reductant. Monobromobimane was added to the solution and allowed to react for 20 min in the dark. Addition of acetic acid stopped the derivatization reaction. The sample was injected onto a reverse-phase 5 μm (4.6 × 75 mm) column. Derivatized glutathione was eluted from the column by a linear gradient of 5%–14.2% methanol.

DTNB Assay

The DTNB assay was performed as described previously [35]. Cells were grown in LB to the desired growth stage, centrifuged, and suspended in PBS. The optical density was normalized to 4.0 for all cell samples. The cell suspensions were passaged twice through a French pressure cell. A solution of 5-5′-dithiobis-2-nitrobenzoate (DTNB) (4 mg/ml) was prepared in ethanol. Cell lysate (1 ml) and DTNB solution (20 μl) were mixed together and allowed to react at room temperature for 20 min. The absorbance of the solution at 412 nm was measured, and the thiol concentration was calculated.

Elemental Analysis

Cells were grown to the desired growth stage, centrifuged, and suspended in PBS. The optical density was normalized to $OD = 4.0$, corresponding to 4×10^9 cells, for all samples. Then, the cells were washed once and resuspended in PBS. The cells suspensions

were passaged twice through a French pressure cell. Sulfur analysis of the samples was performed at Severn Trent Laboratories (Austin, TX) using inductively coupled plasma mass spectrometry.

Electron Microscopy

The JEOL 2010F electron microscope was operated at an accelerating voltage of 200 kV in different modes including conventional TEM, electron diffraction (ED), high-resolution TEM (HRTEM), scanning TEM (STEM), and high-resolution energy dispersive spectroscopy (EDS). High Angle Annular Dark Field (HAADF) microscopy was carried out under STEM mode. The HAADF signal is primarily formed by electrons that have undergone Rutherford backscattering [43]. Therefore, the image contrast is related to composition, with intensity proportional to the square of the atomic number [44]. As a good approximation, lighter elements in HAADF images appear dark and heavier elements appear bright. EDS elemental mapping was performed under ADF STEM mode with a large scanning electron probe size (3 nm) to ensure a high EDS signal-to-noise ratio. To ensure the spatial correspondence between the EDS pattern and the bacteria STEM image, the image rotation between STEM mode and EDS mode was calibrated by using a Gatan (Pleasanton, CA) digital micrograph while STEM images were acquired.

Acknowledgments

We acknowledge the use of the core microscopy facilities in the Texas Materials Institute, Center for Nano- and Molecular Science and Technology, and the Institute for Cellular and Molecular Biology at the University of Texas. This work was supported by the Texas Advanced Research Program, the Welch Foundation, the Packard Foundation, and a National Defense Science and Engineering Graduate Fellowship (to R.Y.S.), the University of Texas College of Engineering Thrust 2000 Robert L. and Jane G. Mitchell Endowed Graduate Fellowship in Engineering (to J.L.B.), and a National Science Foundation Graduate Research Fellowshp (to J.L.B.).

Received: May 26, 2004
Revised: August 26, 2004
Accepted: August 31, 2004
Published: November 29, 2004

References

1. Jaiswal, J.K., Mattoussi, H., Mauro, J.M., and Simon, S.M. (2003). Long-term multiple color imaging of live cells using quantum dot bioconjugates. Nat. Biotechnol. *21*, 47–51.
2. Chan, W.C.W., Maxwell, D.J., Gao, X.H., Bailey, R.E., Han, M.Y., and Nie, S.M. (2002). Luminescent quantum dots for multiplexed biological detection and imaging. Curr. Opin. Biotechnol. *13*, 40–46.
3. Brown, K.R., Lidar, D.A., and Whaley, K.B. (2002). Quantum computing with quantum dots on quantum linear supports. Phys. Rev. A *65*. 10.1103/PhysRevA.65.012307.
4. Murray, C.B., Kagan, C.R., and Bawendi, M.G. (2000). Synthesis and characterization of monodisperse nanocrystals and close-packed nanocrystal assemblies. Annu. Rev. Mater. Sci. *30*, 545–610.
5. Whitling, J.M., Spreitzer, G., and Wright, D.W. (2000). A combinatorial and informatics approach to CdS nanoclusters. Adv. Mater. *12*, 1377–1380.
6. Belcher, A.M., Wu, X.H., Christensen, R.J., Hansma, P.K., Stucky, G.D., and Morse, D.E. (1996). Control of crystal phase switching and orientation by soluble mollusc-shell proteins. Nature *381*, 56–58.
7. Blakemore, R. (1975). Magnetotactic bacteria. Science *190*, 377–379.
8. Schmid, G. (1992). Large clusters and colloids: Metals in the embryonic state. Chem. Rev. *92*, 1709–1727.
9. Henglein, A. (1989). Small-particle research: Physicochemical properties of extremely small colloidal metal and semiconductor particles. Chem. Rev. *89*, 1861–1873.
10. Bae, W.O., Abdullah, R., Henderson, D., and Mehra, R.K. (1997). Characteristics of glutathione-capped ZnS nanocrystallites. Biochem. Biophys. Res. Commun. *237*, 16–23.
11. Bae, W., and Mehra, R.K. (1998). Properties of glutathione- and phytochelatin-capped CdS bionanocrystallites. J. Inorg. Biochem. *69*, 33–43.
12. Bae, W., and Mehra, R.K. (1998). Cysteine-capped ZnS nanocrystallites: Preparation and characterization. J. Inorg. Biochem. *70*, 125–135.
13. Bae, W., Abdullah, R., and Mehra, R.K. (1998). Cysteine-mediated synthesis of CdS bionanocrystallites. Chemosphere *37*, 363–385.
14. Yu, W.W., Wang, Y.A., and Peng, X.G. (2003). Formation and stability of size-, shape-, and structure-controlled CdTe nanocrystals: Ligand effects on monomers and nanocrystals. Chem. Mater. *15*, 4300–4308.
15. Qu, L.H., Peng, Z.A., and Peng, X.G. (2001). Alternative routes toward high quality CdSe nanocrystals. Nano Lett. *1*, 333–337.
16. Douglas, T., Strable, E., Willits, D., Aitouchen, A., Libera, M., and Young, M. (2002). Protein engineering of a viral cage for constrained nanomaterials synthesis. Adv. Mater. *14*, 415.
17. Douglas, T., and Young, M. (1998). Host-guest encapsulation of materials by assembled virus protein cages. Nature *393*, 152–155.
18. Shenton, W., Douglas, T., Young, M., Stubbs, G., and Mann, S. (1999). Inorganic-organic nanotube composites from template mineralization of tobacco mosaic virus. Adv. Mater. *11*, 253.
19. Mao, C.B., Flynn, C.E., Hayhurst, A., Sweeney, R., Qi, J.F., Georgiou, G., Iverson, B., and Belcher, A.M. (2003). Viral assembly of oriented quantum dot nanowires. Proc. Natl. Acad. Sci. USA *100*, 6946–6951.
20. Flynn, C.E., Mao, C.B., Hayhurst, A., Williams, J.L., Georgiou, G., Iverson, B., and Belcher, A.M. (2003). Synthesis and organization of nanoscale II-VI semiconductor materials using evolved peptide specificity and viral capsid assembly. J. Mater. Chem. *13*, 2414–2421.
21. Mao, C.B., Solis, D.J., Reiss, B.D., Kottmann, S.T., Sweeney, R.Y., Hayhurst, A., Georgiou, G., Iverson, B., and Belcher, A.M. (2004). Virus-based toolkit for the directed synthesis of magnetic and semiconducting nanowires. Science *303*, 213–217.
22. Dameron, C.T., Reese, R.N., Mehra, R.K., Kortan, A.R., Carroll, P.J., Steigerwald, M.L., Brus, L.E., and Winge, D.R. (1989). Biosynthesis of cadmium sulphide quantum semiconductor crystallites. Nature *338*, 596–597.
23. Mehra, R.K., and Winge, D.R. (1991). Metal ion resistance in fungi: molecular mechanisms and their regulated expression. J. Cell. Biochem. *45*, 30–40.
24. Vido, K., Spector, D., Lagniel, G., Lopez, S., Toledano, M.B., and Labarre, J. (2001). A proteome analysis of the cadmium response in Saccharomyces cerevisiae. J. Biol. Chem. *276*, 8469–8474.
25. Li, Z.S., Szczypka, M., Lu, Y.P., Thiele, D.J., and Rea, P.A. (1996). The yeast cadmium factor protein (YCF1) is a vacuolar glutathione S-conjugate pump. J. Biol. Chem. *271*, 6509–6517.
26. Li, Z.S., Lu, Y.P., Zhen, R.G., Szczypka, M., Thiele, D.J., and Rea, P.A. (1997). A new pathway for vacuolar cadmium sequestration in Saccharomyces cerevisiae: YCF1-catalyzed transport of bis(glutathionato)cadmium. Proc. Natl. Acad. Sci. USA *94*, 42–47.
27. Dameron, C.T., Smith, B.R., and Winge, D.R. (1989). Glutathione-coated cadmium-sulfide crystallites in Candida glabrata. J. Biol. Chem. *264*, 17355–17360.
28. Dameron, C.T., and Winge, D.R. (1990). Characterization of peptide-coated cadmium-sulfide crystallites. Inorg. Chem. *29*, 1343–1348.
29. Shenton, W., Pum, D., Sleytr, U.B., and Mann, S. (1997). Synthesis of cadmium sulphide superlattices using self-assembled bacterial S-layers. Nature *389*, 585–587.
30. Wang, C.L., Lum, A.M., Ozuna, S.C., Clark, D.S., and Keasling, J.D. (2001). Aerobic sulfide production and cadmium precipitation by Escherichia coli expressing the Treponema denticola cysteine desulfhydrase gene. Appl. Microbiol. Biotechnol. *56*, 425–430.
31. Wang, C.L., Michels, P.C., Dawson, S.C., Kitisakkul, S., Baross, J.A., Keasling, J.D., and Clark, D.S. (1997). Cadmium removal

by a new strain of Pseudomonas aeruginosa in aerobic culture. Appl. Environ. Microbiol. *63*, 4075–4078.
32. Lins, U., and Farina, M. (1998). Magnetosome size distribution in uncultured rod-shaped bacteria as determined by electron microscopy and electron spectroscopic imaging. Microsc. Res. Tech. *42*, 459–464.
33. Klaus, T., Joerger, R., Olsson, E., and Granqvist, C.G. (1999). Silver-based crystalline nanoparticles, microbially fabricated. Proc. Natl. Acad. Sci. USA *96*, 13611–13614.
34. Williams, D.B., and Carter, C.B. (1996). Transmission Electron Microscopy (New York: Plenum Press).
35. Ellman, G.L. (1959). Tissue sulfhydryl groups. Arch. Biochem. *82*, 70–77.
36. Ahmad, A., Mukherjee, P., Mandal, D., Senapati, S., Khan, M.I., Kumar, R., and Sastry, M. (2002). Enzyme mediated extracellular synthesis of CdS nanoparticles by the fungus, Fusarium oxysporum. J. Am. Chem. Soc. *124*, 12108–12109.
37. Kowshik, M., Vogel, W., Urban, J., Kulkarni, S.K., and Paknikar, K.M. (2002). Microbial synthesis of semiconductor PbS nanocrystallites. Adv. Mater. *14*, 815–818.
38. Blattner, F.R. (1996) *E. coli* Genome Project (http://www.genome.wisc.edu/).
39. Rao, N.N., and Kornberg, A. (1996). Inorganic polyphosphate supports resistance and survival of stationary-phase Escherichia coli. J. Bacteriol. *178*, 1394–1400.
40. Castuma, C.E., Huang, R., Kornberg, A., and Reusch, R.N. (1995). Inorganic polyphosphates in the acquisition of competence in Escherichia coli. J. Biol. Chem. *270*, 12980–12983.
41. Nossal, N.G., and Heppel, L.A. (1966). The Release of enzymes by osmotic shock from Escherichia coli in exponential phase. J. Biol. Chem. *13*, 3055–3062.
42. Anderson, M.E. (1985). Determination of glutathione and glutathione disulfide in biological samples. Methods Enzymol. *113*, 548–555.
43. Crewe, A.V. and Wall, J. (1970). A scanning microscope with 5 Å resolution. J. Mol. Biol. *48*, 375–393.
44. Pennycooke, S.J. and Jesson, D.E. (1991). High resolution Z-contrast imaging of crystals. Ultramicroscopy *37*, 14–38.